Earthquakes and Structures, *Vol. 6, No. 6 (2014) 627-646*
DOI: http://dx.doi.org/10.12989/eas.2014.6.6.627

Numerical simulation of an adobe wall under in-plane loading

Tarque Nicola*[1], Camata Guido[2a], Varum Humberto[3b], Spacone Enrico[2c] and Blondet Marcial[1d]

[1]*Department of Engineering, Division of Civil Engineering, Pontificia Universidad Católica del Perú, Av. Universitaria 1801, Lima 32, Peru*
[2]*Department of Engineering and Geology, University 'G. D'Annunzio' Chieti-Pescara. Viale Pindaro 42, 65127 Pescara, Italy*
[3]*Department of Civil Engineering, University of Aveiro. 3810-193, Aveiro, Portugal*

(Received October 30, 2013, Revised February 5, 2014, Accepted March 3, 2014)

Abstract. Adobe is one of the oldest construction materials that is still used in many seismic countries, and different construction techniques are found around the world. The adobe material is characterized as a brittle material; it has acceptable compression strength but it has poor performance under tensile and shear loading conditions. Numerical modelling is an alternative approach for studying the nonlinear behaviour of masonry structures such as adobe. The lack of a comprehensive experimental database on the adobe material properties motivated the study developed here. A set of a reference material parameters for the adobe were obtained from a calibration of numerical models based on a quasi-static cyclic in-plane test on full-scale adobe wall representative of the typical Peruvian adobe constructions. The numerical modelling, within the micro and macro modelling approach, lead to a good prediction of the in-plane seismic capacity and of the damage evolution in the adobe wall considered.

Keywords: adobe masonry; material properties; in-plane behaviour; seismic capacity; numerical modelling

1. Introduction

In many developing countries earthen dwellings are traditional residential solutions because soil is abundant, readily available and free. Unfortunately these countries are also regions of high seismicity (Fig. 1). In the majority of the cases, these adobe buildings are built by the owners during work campaigns in their neighbourhood without taking into account specific seismic reinforcements. Adobe dwellings are built with sun dried mud blocks and mud mortar. To form the wall, the adobe bricks run horizontally with the greater dimension parallel to the wall surface (stretcher way) or with the greater dimension perpendicular to the wall surface (header way) with mud mortar between them, forming the bed and head joints. The adobe dwellings have excellent

*Corresponding author, Associate Professor, E-mail: sntarque@pucp.edu.pe
[a]Assistant Professor, E-mail: g.camata@unich.it
[b]Associate Professor, E-mail: hvarum@ua.pt
[c]Professor, E-mail: espacone@unich.it
[d]Professor, E-mail: mblondet@pucp.pe

 ISSN: 2092-7614 (Print), 2092-7622 (Online)

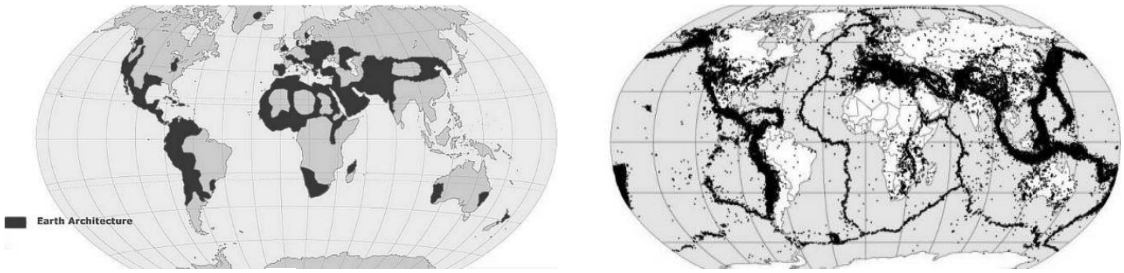

(a) (b)

Fig. 1 Earthen constructions around the world, (a) distribution of earthen constructions (from De Sensi 2003), (b) distribution of earthquake epicenters (from Lowman and Montgomery 1998)

Fig. 2 Typical in-plane damage in adobe walls.

acoustic and thermal characteristics. Due the adobe thermal mass, these buildings are warm during winter and are fresh and cool during summer. However, their seismic performance is extremely poor due to a perverse combination of its mechanical properties: relatively high density, extremely low tensile strength, and brittle failure mode. Every time a strong earthquake occurs, there is widespread damage, economic losses and casualties due to collapse of earthen houses.

Understanding the seismic behaviour and capacity of earthen structures is a first step toward reducing their seismic vulnerability. Experimental tests are the primary source of information; however, they are costly and not necessarily available due to limited laboratory capacities, specifically in developing countries. Numerical modelling is a valid alternative for evaluating the seismic behaviour of masonry buildings (e.g. Gambarotta and Lagomarsino 1997; Lourenço 1996; Magenes and Della Fontana 1998; Stavridis and Shing 2010; Roca *et al*. 2010; Pelà *et al*. 2013).Adobe walls have a very low tensile strength, thus cracks typically initiate in zones subjected to higher tensile stresses, such as corners of doors and windows. Usually, vertical cracks start at the connection of perpendicular walls due to the high stress concentration and lack of confinement elements. Furthermore, horizontal cracks may form close to the façade base allowing it to overturn due to out-of-plane demands. The typical crack pattern due to in-plane shear forces is X-diagonal shaped, as shown in Fig. 2. Tarque *et al*. (2012) shows some limit states and displacement capacities of adobe walls subjected to in-plane and out-of-plane loads, which are useful to study the seismic vulnerability of adobe buildings based on a mechanics-based procedure. According to Webster (2008), the cracking due to in-plane forces are not particularly

serious unless the relative displacement across them becomes large, thus initiating the out-of-plane overturning of the small wall blocks formed by the cracks.

For adobe structures, the brick and mortar joints are made of similar materials, mainly soil. Therefore, as a first approximation and without loss of accuracy, it seems reasonable to treat the adobe masonry as a homogeneous material. The state-of-the-art for the numerical modelling of unreinforced masonry point to two main approaches within the finite element method: discrete modelling and smeared crack modelling. Another approach consists in idealizing the structure through an equivalent frame where each wall is discretized by a set of masonry panels (piers and spandrels) in which the non-linear response is concentrated (Lagomarsino *et al.* 2013; Calderini and Lagomarsino 2008; Magenes and Della Fontana 1998). The piers and spandrels are connected by rigid joint connections. The smeared crack modelling and the equivalent frame modelling are macro-modelling approaches; while the discrete approach is considered as part of the micro-modelling. For adobe masonry, the lack of information and experimental data concerning some of the material properties, particularly in the inelastic range, makes numerical modelling more uncertain. Therefore, this work focuses on the calibration of the material properties of an adobe wall cyclically tested until its collapse in order to numerically reproduce its structural behaviour.

This paper presents the results obtained with three different numerical models developed to represent experimental tests carried out at the Pontifical Catholic University of Peru (PUCP). The models are developed in two finite element programme following a simplified discrete and a smeared cracking approach.

2. Experimental test on an adobe wall

Blondet *et al*. (2005) carried out a displacement controlled cyclic test (push-pull) on a typical adobe wall at the PUCP. The test intended to analyse the wall cyclic response and the damage pattern evolution due to in-plane forces. The wall had an H-shape configuration (Fig. 3a), where the main longitudinal wall (with a central window opening) was 3.06 m long, 1.93 m high and 0.30 m thick. The wall had two 2.48 m long transverse walls that were intended to: a) simulate the influence of the connection with the transversal walls found in typical buildings; b) avoid rocking due to in-plane actions. The brick composition for the adobe was soil, coarse sand and straw in proportion 5/1/1 in volume, and for the mud mortar, 3/1/1. The soil was basically obtained from a farm field, the coarse sand diameter was from 0.5 to 1 mm and the straw was dry grass.

The specimen was built over a reinforced concrete continuous foundation beam. A reinforced concrete ring beam was built at the top of the adobe wall simulating the gravity loads applied by traditional Peruvian roof made of wooden beams, canes, straw, mud and corrugated zinc sheets. The weight of this ring beam was around 16 kN, allowing to have a distributed load of 2.07 kN/m. Neither additional of vertical loads nor control of the variation was imposed to the system during the test. The ring beam also ensured a more uniform distribution of the horizontal displacements applied to the wall. The window lintel was made of wood.

The horizontal displacement loadwas applied in a series of loading cycles with increasing peak displacements at the top concrete beam through a servo-hydraulic actuator fixed to a rigid steel reaction frame (see left top side of Fig. 3a). The top peak displacements were 0.5, 1, 2, 5, 10 and 20 mm; however, the last peak value was not considered for the numerical analyses because it was associated to unstable sliding wall behaviour. The displacements were applied slowly in order to

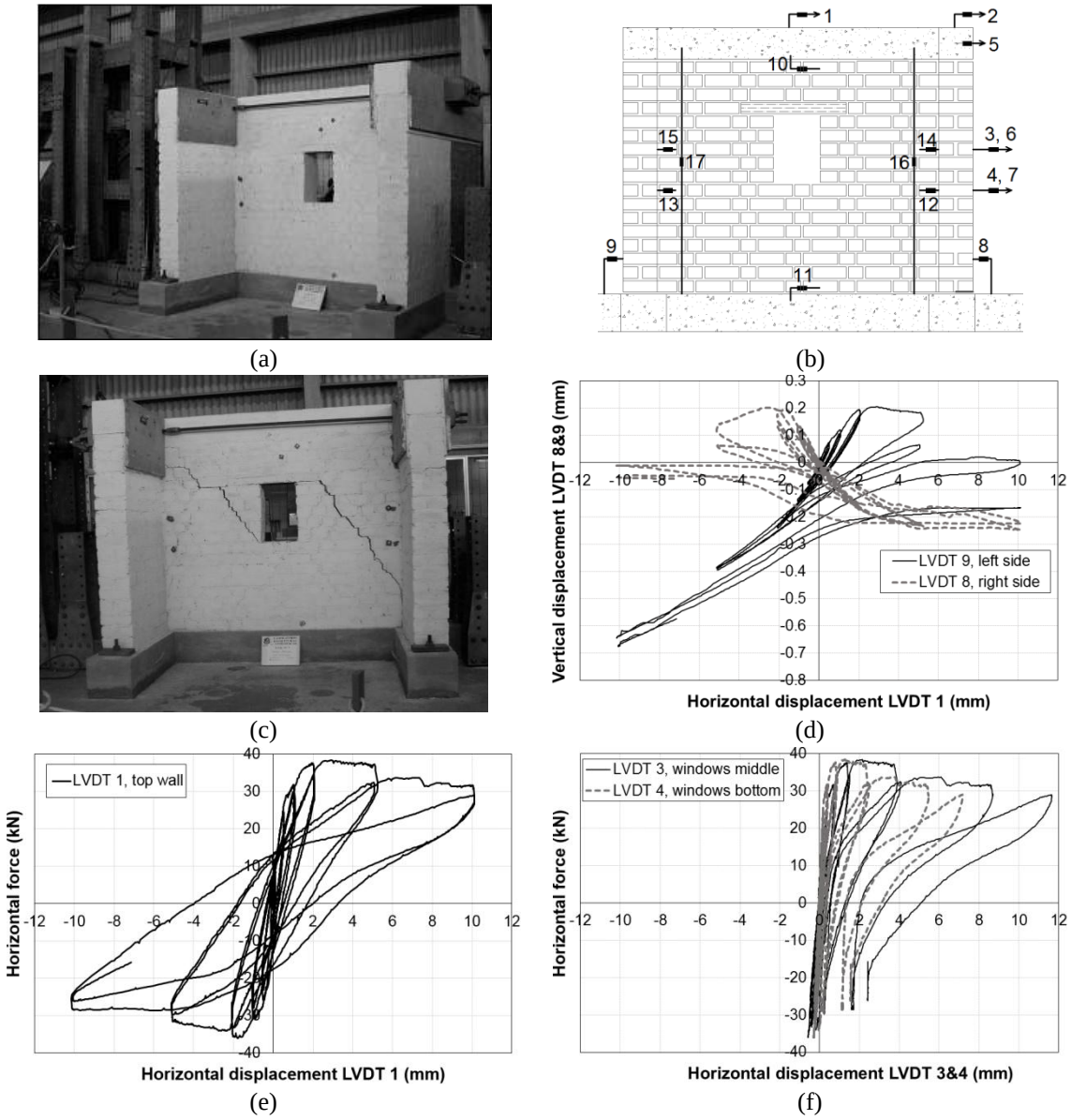

Fig. 3 Adobe wall tested at PUCP. (a) front side of the adobe wall, (b) distribution of LVDT, rear side of the adobe wall, (c) damage pattern evolution during the cyclic test, (d) vertical displacements LVDT 9 and 8, (e) horizontal displacement at the wall top LVDT 1, (f) horizontal displacement at the middle (LVDT 3) and bottom (LVDT 4) part of the window (Blondet *et al.* 2005)

avoid dynamic effects, the velocity values were 0.5 mm/min, 1 mm/min; 2 mm/min; 5 mm/min; 10 mm/min and 20 mm/min corresponding to each peak displacement.A total of 17 Linear Variable Displacement Transducers (LVDT) were placed in the opposite side of the front wall (Fig. 3b).

During the test the cracks started between 1 and 2 mm top displacement at the windows corners

and evolved diagonally up to the top and to the base of the wall. The maximum wall strength was reached around 2 mm top displacement, after that a clear strength reduction was registered. During reversal loads, the cracks generated the typical X-shape cracks due to in-plane forces; however, some unsymmetrical cracking is observed in Fig. 3c which were generated due to the position of the load application (left top wall) and sequence of degradation in the adobe wall for cyclic loads (first cracking start from top left to right bottom parts). At 5 mm top displacement large horizontal fissures appeared at the transversal walls and vertical fissures at the intersection of longitudinal and transversal walls, with increment of diagonal cracking in the main wall (Fig. 3c).

For 10 mm top displacement cycle a notable loss of lateral strength in the wall was observed with an increment of crack width and tensile cracking in the adobe bricks. The diagonal cracking in both directions continue growing in thickness. Horizontal cracks appeared at the base of the transversal walls, allowing a major sliding mechanism of the walls. At this stage, some rigid blocks were identified.

Fig. 3d shows the vertical displacement measured by the LVDT 8 and 9 at the centreline of the two end wall. The positive vertical displacement indicates crack opening measured by LVDT 9 or 8 in the first three adobe rows; while negative values indicates crack closing, crushing and some sliding in the material. Positive horizontal displacements in Fig. 3d and 3e indicate that the top displacement goes from left to right; while negative horizontal displacements indicates the contrary, in both cases the horizontal displacement is referred to LVDT 1. In Fig. 3d is seen that for pushing loads a complete opening of cracking occurs after 2 mm top displacement at the left wall side with some sliding in the right wall side due to horizontal fissures. The difference in the vertical values of LVDT 8 and 9 indicates a non-symmetrical vertical response at the two end walls due to some rotation at the top concrete beam during the load application and the separation of the complete wall into a number of rigid parts.

A comparison of Fig. 3e and 3f shows that the maximum deformation is seen at the windows level, where the displacement exceeds the 10 mm top displacement. In particular for Fig. 3f (LVDT 3 and 4 placed at the right wall side) can be understood from the almost null negative displacements that the wall is divided into blocks and its movement is controlled by the opening, closing and sliding phenomenon of cracking.

3. Masonry models within the finite element method

Previous research results have shown that the response of masonry structures up to failure can be successfully modelled using techniques applied to concrete mechanics (Lotfi and Shing 1994). According to Lourenço (1996), the numerical modelling of masonry walls within the finite element method can follow either the micro-modelling of each of its components (discontinuous or discrete approach) or the macro-modelling of the wall (continuum approach), thus assuming that the masonry wall is homogeneous. More specifically, the following approaches, illustrated in Fig. 4, can be described as:

- detailed-micro modelling. Bricks and mortar joints are discretized using continuum elements, with the brick-mortar interface represented by discontinuous elements;
- simplified micro-modelling. The bricks are modelled as continuum elements, while the behaviour of the mortar joints and of the brick-mortar interface are lumped in discontinuous elements;

- macro-modelling. Bricks, mortar and brick-mortar interface are smeared out and the masonry is treated as a continuum.

The first two modelling techniques are considered part of the discontinuous/discrete approach, where the failure zones are placed in pre-defined weak paths, such as the mortar joints or brick. The detailed and simplified micro-modelling approaches are computationally expensive for the analysis of large masonry structures; however, they represent important research tools that can be used as an alternative to costly and often time-consuming laboratory experiments (Giordano *et al*. 2002), provided adequate material data and precise and reliable constitutive models are available. The third modelling technique performs well in cases where the damage zones are spread over the wall, and not limited to few bricks and mortar joints. In the present paper, both the discrete and continuum approaches are used to calibrate the material properties and to reproduce the response of the adobe wall described in the previous section and tested at the PUCP.

4. Finite element approaches for crack modelling

4.1 Discontinuous approach

The discontinuous approach, such as the discrete crack model introduced by Ngo and Scordelis (1967) was first proposed to model the concrete. It assumes discontinuous elements interacting with material cracks represented as boundaries with zero thickness.

The simplified micro-model of Fig. 4c is considered a discontinuous model, where the inelasticity in the mortar and in the brick-mortar interface is lumped in a discrete brick-brick interface. Lourenço (1996) developed a model where brick elements are elastic and are connected by an inelastic composite interface model. This interface model is capable of describing different failure modes, such as cracking of the mortar, sliding along the bed or head joints at low values of normal stress, and crushing at the brick-mortar joints (Fig. 5).

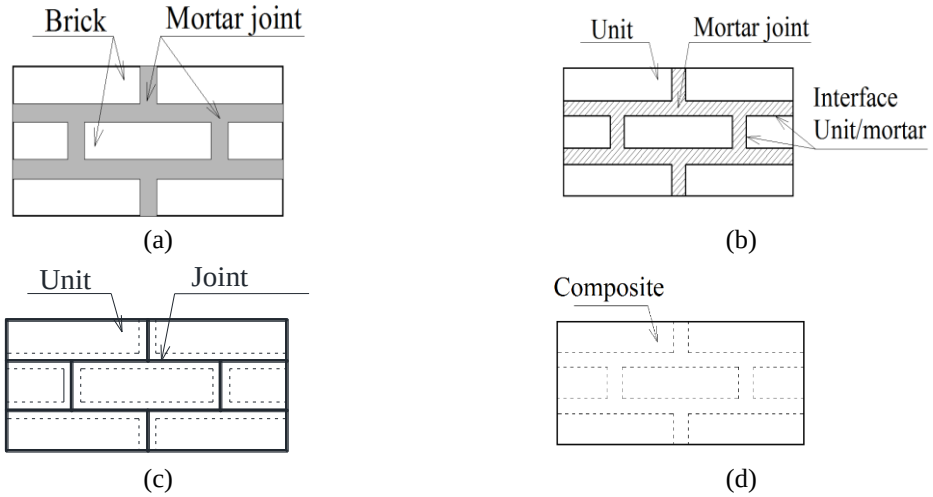

Fig. 4 Modelling strategies for masonry structures, (a) masonry sample, (b) detailed micro-modelling, (c) simplified micro-modelling, (d) masonry sample (modified from Lourenço 1996)

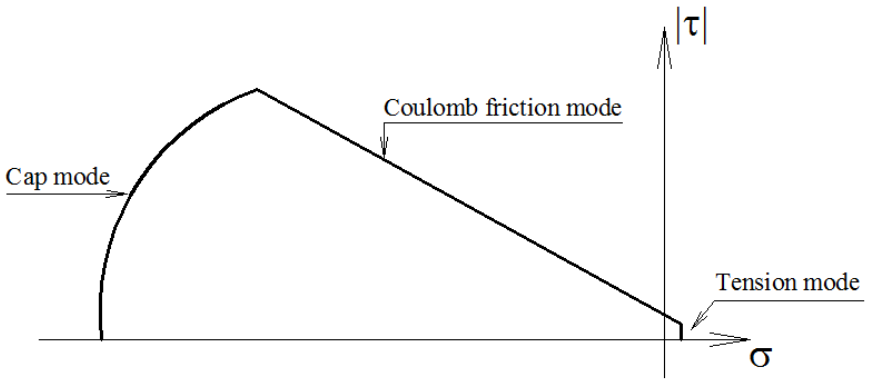

Fig. 5 Constitutive model proposed by Lourenço (1996) based on plasticity concepts.

The composite interface model of Fig. 5, also referred to as combined cracking-shearing-crushing model, is based on the plasticity theory. The main input data for this model are the constitutive laws for the tension, shear and compression behaviour of the composite interface model (Fig. 6). In these laws the primary variable is the fracture energy, which is the area under the monotonic stress-displacement curve after the peak.

4.1 Continuum approach

The smeared crack model uses continuum elements where the concrete/masonry cracks are assumed smeared and distributed over the elements. The fracture process is initiated when the maximum principal stress at an integration point exceeds the material strength. The crack propagation is mainly controlled by the shape of the softening diagram and the material fracture energy (Cruz *et al*. 2004). The tensile and compressive constitutive laws are the main input data for the smeared crack model, as well as the fracture energy for each of them (see Figs. 6 and 7).

Two approaches are typically followed for the formulation of the smeared crack model: the decomposed-strain model and the total-strain model. The decomposed-strain modelsplits the total strain into the sum of the material strain plus the crack strain. The material strain accounts for the elastic strain, the plastic strain, the creep strain, the thermal strain, *etc*. The crack strain describes the deformations due to crack opening only. The total strain model makes use of the total tensile and compressive hardening/softening curve of the masonry in terms of stress versus strain.

4.2.1 Smeared crack model

The smeared crack model uses continuum elements where the concrete/masonry cracks are assumed smeared and distributed over the elements. The fracture process is initiated when the maximum principal stress at an integration point exceeds the material strength. The crack propagation is mainly controlled by the shape of the softening diagram and the material fracture energy (Cruz *et al*. 2004). The tensile and compressive constitutive laws are the main input data for the smeared crack model, as well as the fracture energy for each of them (see Figs. 6 and 7).

Two approaches are typically followed for the formulation of the smeared crack model: the decomposed-strain model and the total-strain model. The decomposed-strain modelsplits the total strain into the sum of the material strain plus the crack strain. The material strain accounts for the

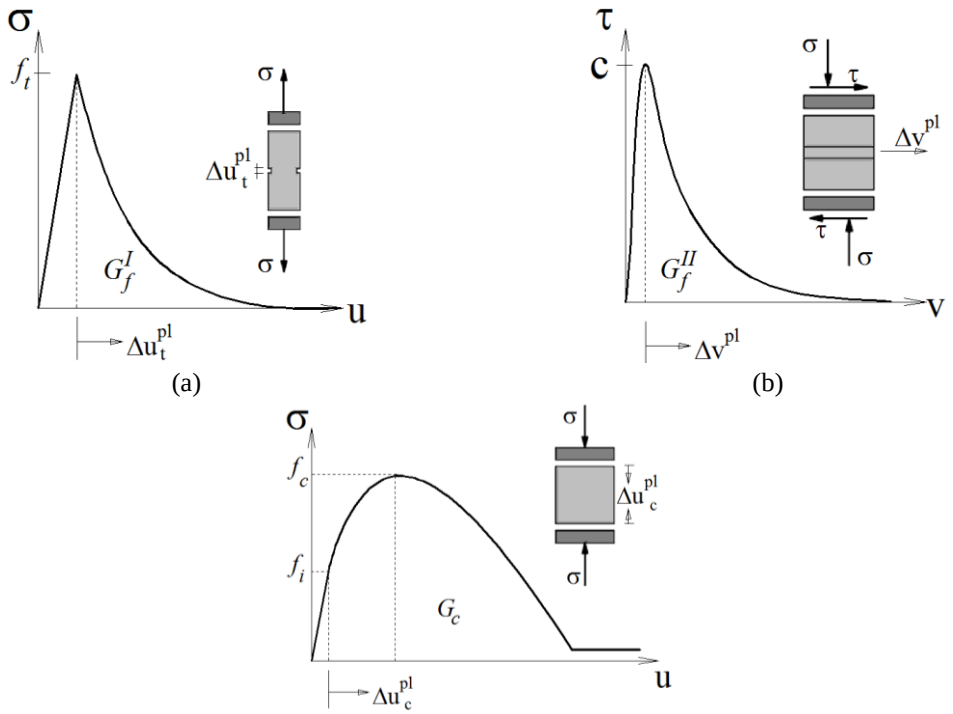

Fig. 6 (Continuation) Stressdisplacement diagrams for quasi brittle materials, (a) tensile behaviour for mortar joints, (b) shear behaviour for mortar joints, (c) compressive behaviour of brick and mortar joints

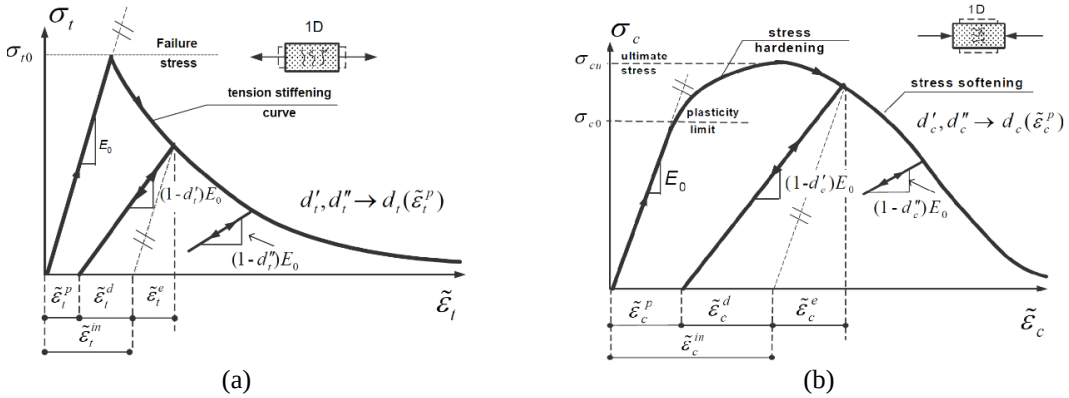

Fig. 7 Response of concrete under tensile and compressive loads implemented in Abaqus for the concrete damaged plasticity model, (a) tensile behaviour, (b) compressive behaviour (modified from Wawrzynek and Cincio 2005)

elastic strain, the plastic strain, the creep strain, the thermal strain, etc. The crack strain describes the deformations due to crack opening only. The total strain model makes use of the total tensile and compressive hardening/softening curve of the masonry in terms of stress versus strain.

4.2.2 Plastic-damage based model

The plastic-damage model is based on the work developed by Lubliner *et al*. (1989) and later extended by Lee and Fenves (1998). This model is a continuum, plastic-based, damage model for concrete, where the two main failure mechanisms are tensile cracking and compressive crushing of the material. This model assumes that failure of concrete (or unreinforced masonry in this work) can be effectively modelled using its uniaxial tensile, uniaxial compressive and plasticity characteristics. Unlike the smeared crack models, the cracking in the damage-plastic based model is represented by the damage factors (*dt*, *dc*) that reduce the modulus of elasticity in tension and compression for reversal loading (Fig. 7). In contrast to the classical theory of plasticity, the damaged plasticity model uses a set of variables that alters the elastic and plastic behaviour.

5. Finite element models of the adobe wall:analysis and comparison

5.1 Monotonic seismic response

The adobe wall tested by Blondet *et al*. (2005), Fig. 3, is modelled using three finite element approaches described before, i.e.,: the discrete simplified micro-model, the continuum approach within the total-strain model and the continuum approach within the concrete damaged plasticity model. The first two models are analysed with Midas FEA, the former using solid elements and the second using shell elements. The last model is analysed with Abaqus/Standard using shell elements. In all cases the geometric nonlinearity is taken into account. The configurations of the numerical models are shown in Fig. 8.

All models include the top and base reinforced concrete beams, the adobe walls and the timber lintel. The base was fully fixed. Since the experimental test was displacement-controlled, a monotonic top displacement was applied to the numerical model at one vertical edge of the top concrete beam up to a maximum displacement of 10 mm. In this first part, just a monotonic displacement is considered for the calibration of material parameters. At higher displacement levels, wall instability started during the experimental test and though the test was not interrupted, the results beyond 10 mm were not considered reliable (Blondet *et al*. 2005).

The loading sequence in the numerical monotonic analysis is as follows: the gravity loads are applied first, followed by imposed horizontal displacements. As in the tests, the top concrete beam is free to have vertical displacements due to geometric non linearity and deformation of the adobe material. In Midas FEA, the lateral displacement is imposed incrementally following the arc-length iterative procedure in combination with the initial stiffness. The convergence criterion is controlled through a displacement and energy norm ratios of 0.005 and 0.01, respectively. In Abaqus/Standard, the top-displacement is imposed following a full Newton-Raphson iterative procedure. An automatic stabilization is selected for the convergence criterion, with a specified dissipated energy fraction of 0.001 and an adaptive stabilization with maximum ratio of stabilization to strain energy of 0.01. In both software platforms the nonlinear geometric effects are considered.

As previously mentioned, a complete database of material properties for adobe bricks and walls used in Peru is not available. The scarce available data refers to compressive strength and elastic

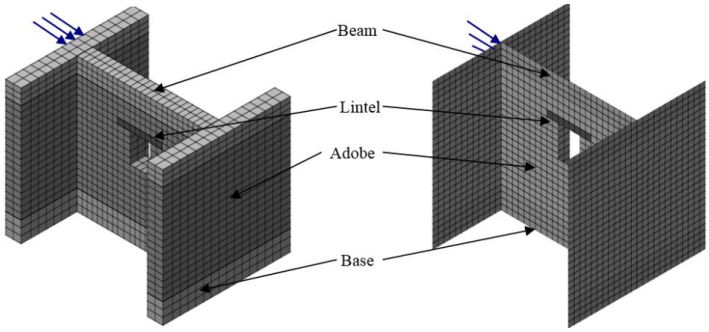

(a) (b)

Fig. 8 Numerical models of the tested adobe wall, (a) model in Midas FEA (solid elements), (b) model in Midas FEA and Abaqus/Standard (shell elements)

properties only (e.g. modulus of elasticity). The lack of data for defining the inelastic properties of adobe, such as the fracture energy in compression and tension, should be obtained through an appropriate experimental campaign. However, in this study an approximation of these inelastic parameters is obtained through a correlation study betweenthe global experimental and numerical results of the adobe wall tested at the PUCP. These numerical material values should be considered as a mere reference for other analyses since additional experimental tests are needed to obtain the mechanical properties of different adobe materials (whose strength changes, for example, depending on the soil type) and building techniques.

5.1.1 Discrete approach: composite interface model

The adobe bricks, the concrete beams and the lintel are modelled using 8-node hexahedron (solid) elements with elastic and isotropic material properties. The elastic properties of the different materials are shown in Table 1. E is the modulus of elasticity and was calibrated based on Blondet and Vargas (1978) to match the initial stiffness measured in the experimental test; υ is the Poisson's ratio, γ_m is the weight density. The crack propagation (inelasticity) follows the mortar joints, which are modelled using the three dimensional combined interface model with 4 integration points. This interface model is based on the model proposed by Lourenço (1996).

Table 2 shows the calibrated material parameters used for the combined interface model. k_n is the normal stiffness modulus, k_t is the shear stiffness modulus, c is the cohesion, φ_o is the frictional angle, ψ is the dilatancy angle, φ_r is the residual friction angle, f_t is the tensile strength, G^I_f is the fracture energy for Mode I (related to the tensile softening), a and b are factors to evaluate the fracture energy for Mode II (computed as $G^{II}_f = a(\sigma+b)$ and related to the shear behaviour). In MIDAS FEA the compression cap is not implemented when dealing 3D interface model, so in this model the compression for the mortar is elastic; however, as it is explained later the in-plane behaviour of the adobe wall is less influence by its compressive strength.

The earth mortar properties, marked with * in Table 2, were calibrated based on the experimental results and observations, namely the pushover envelope curve and the observed damages and failure pattern of the tested adobe wall. The softening curve in tension (exponential) follows the same shapes specified by Lourenço (1996) for clay masonry, with lower strength characteristics typically for adobe masonry.

The damage pattern and displaced configuration at the end of the analysis are shown in Fig. 9.

Table 1 Elastic material properties

Adobe blocks			Concrete			Timber		
E (MPa)	υ	γ_m (N/mm^3)	E (MPa)	υ	γ_m (N/mm^3)	E (MPa)	υ	γ_m (N/mm^3)
230	0.2	2e-05	22000	0.25	2.4e-05	10000	0.15	6.87e-06

Table 2 Material properties for the interface model (mortar joints)

Structural						Mode I		Mode II	
k_n (N/mm^3)*	k_t (N/mm^3)*	c (N/mm^2)	φ_o (deg)	Ψ (deg)	φ_r (deg)	f_t (N/mm^2)*	G_f^I (N/mm)*	a (mm)*	b (N/mm)*
8	3.2	0.05	30	0	30	0.01	0.0008	0	0.01

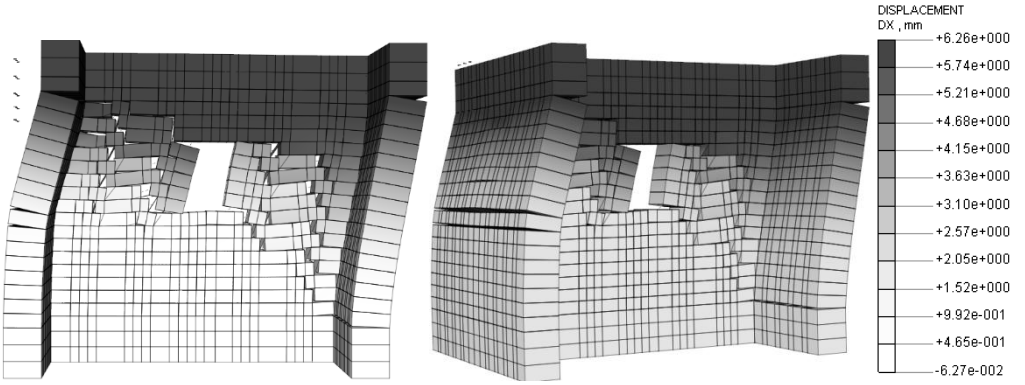

Fig. 9 Deformation pattern of the adobe wall considering the combined interface model for a top displacement of 6.2 mm, Midas FEA.

The crack pattern follows the experimental results: the cracks go from the top left (where the displacement is applied) to the bottom right of the wall (Fig. 3). The horizontal cracks in the transversal walls were also observed during the experimental tests. Since the applied load is monotonic, the FE model cannot capture the X-shape crack pattern. The presence of the two transversal walls prevents wall rocking, correctly reproducing the tested wall response. The maximum displacement reached at the top of the wall is around 6.2 mm, thereafter the program stopped due to convergence problems associated to large element distortions.

5.1.2 Continuum approach

Total-strain model

First order shell elements are used in the finite element model created in Midas FEA. The model uses rectangular 4-node shell elements. The element size is about 100 × 100 mm; which ends on a characteristic element length of 141 mm (diagonal of the element size). The concrete beams and the lintel are represented by elastic and isotropic materials. The adobe masonry (bricks plus mortar), which is defined here as an isotropic material, makes use of the tensile and compressive constitutive laws for representing material inelasticity within the total-strain approach. An exponential function is defined for the tensile behaviour and a parabolic one, similar to the function given by Lourenço (1996), is given for the compressive response. Since experimental data for the softening behaviour in tension and compression is not available, the inelastic strain values are assumed based on the ones for clay masonry and calibrated through the

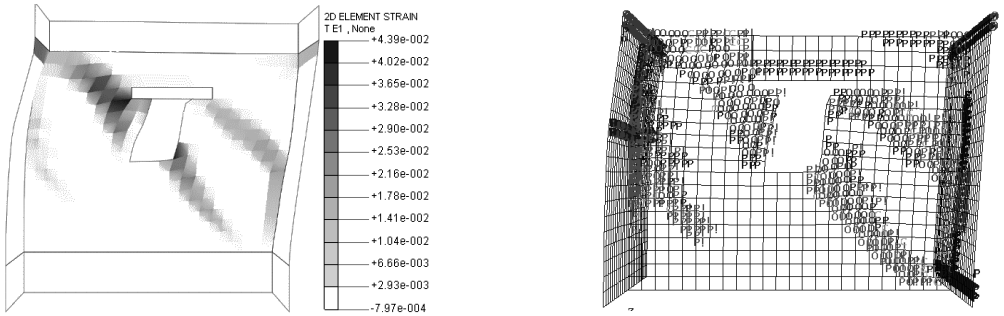

(a) (b)

Fig. 10 (a) Strain (mm/mm) and (b) crack status at the middle surface of the adobe wall considering the total-strain model for a top displacement of 9.38 mm (P: partially open; O: fully open; C: closed)

Table 1 Adobe masonry material properties used for the continuum approach

Elastic				Tension		Compression		
E (N/mm^2)	υ	γ_m (N/mm^3)	h (mm)	f_t (N/mm^2)	G_f^I(N/mm)	f_c (N/mm^2)	G_c (N/mm)	ε_p (mm/mm)
200	0.2	2e-05	141	0.04	0.01	0.45	0.155	0.002

experimental pushover curve. The obtained values are reported in Table 3, where ε_p is the plastic strain related to the maximum compressive strength and h is the characteristic element length.
The modulus of elasticity E of the composite material (adobe plus mortar) was calibrated to match the initial stiffness of the pushover envelope curve obtained from the experimental test. A compressive strength f_c close to 0.70 MPa is specified in the literature (test on adobe piles, Blondet and Vargas 1978), but the complete curve of the uniaxial behaviour law is unavailable. The authors believe that tests on adobe piles don't represent the actual adobe composite behaviour because they consider a portion not representative of the wall. In this work a f_c = 0.45 MPa is specified. Tensile strength and fracture energy are calibrated in this model using the experimental test results, since no data is found in the literature for this type of constructions (adobe). Since a fixed crack model is selected, a reduction of the shear stiffness β = 0.05 was specified for the analysis. The elastic material properties for the concrete and timber are the same as those used in the discrete model presented in Table 1.

Fig. 10 shows the wall strains and crack pattern of the model (e.g. closed, partially open, fully open, *etc*.) at the end of the analysis. The strain pattern is in good agreement with the failure pattern observed in the test (Fig. 3d) if just a monotonic load is assumed. The target maximum displacement was 10 mm. As in the previous model, cracks start at the openings corners and progresses diagonally to the wall edges. Fig. 10a shows that the maximum strains are reached at the contact zone of the wall with the timber lintel and at the corner openings, due to stress concentration in these zones.

Concrete damaged plasticity model

The concrete damaged plasticity model, which accounts for both tensile cracking and compressive crushing, can be effectively applied to masonry too. In this model the effect of material cracking (especially for unloading as for cyclic loadings) is represented through damage factors in tension and compression. As in the previous case, this model is built with rectangular 4

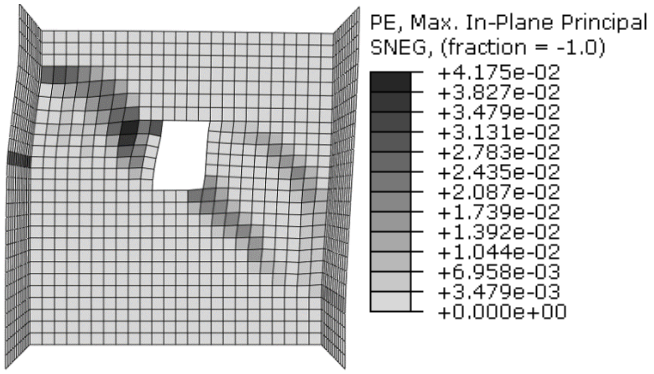

Fig. 11 Maximum plastic strain distribution considering the concrete damaged plasticity model (middle surface) for a top displacement of 10 mm (units of strain in mm/mm), Abaqus/Standard

nodes-shell elements. The size of each element is about 100 × 100 mm. Similarly to the total strain model, the concrete damaged plasticity model defines material inelasticity separately in tension and compression. In Abaqus/Standard, input data is defined based on the material properties presented in Table 3.Fig. 11 shows the damage pattern associated to tensile stresses at the top displacement of 10 mm. The diagonal cracks control the wall behaviour and extend from the opening corners to the wall corners. The largest strains are observed at the contact points between the timber lintel and the wall and at the opening corners (Fig. 11). The horizontal crack pattern at the transversal walls is in agreement with the actual failure pattern observed during the tests.

5.1.3 Comparison of the analytical and experimental results in terms of force displacement curves

The three numerical models reproduced fairly well the monotonic global response of the tested adobe wall, as shown in Fig. 12, as well as the stress distribution and the crack pattern, even though not all analyses reached the maximum imposed displacement of 10 mm due to convergence problems. The material properties (parameters) adopted in these models were obtained from a parametric study changing the parameters one by one (e.g. tensile strength, compression strength, fracture energy, shape of the constitutive laws, etc). The best values were determined by comparison between the numerical with the experimental pushover envelop curve. A correct parametric study should vary all parameters at the same time to look for a non-linear optimization. However, in this work it was not possible due to the great lack of information about the material properties.

When the response of the wall starts being inelastic (approximately at 1 mm top displacement), small differences between the numerical and experimental results are observed. However, as the crack patterns stabilize, all the numerical curves match well the experimental response (after a top displacement of 2 mm, see Fig. 12).

The model with the combined interface law (discrete approach) tends to be more unstable, due to local large deformations in the cracks region, which however describes better the physical discontinuity between the cracks' faces (Fig. 9). Continuum models are more stable because the inelastic properties are smeared in the wall and not concentrated just at the mortar joints, as in the discrete modelling approaches. The first elements that reach the tensile strength are located at the opening and lintel corners, where stress concentration occurs. Also, horizontal cracks appear at the transversal walls.

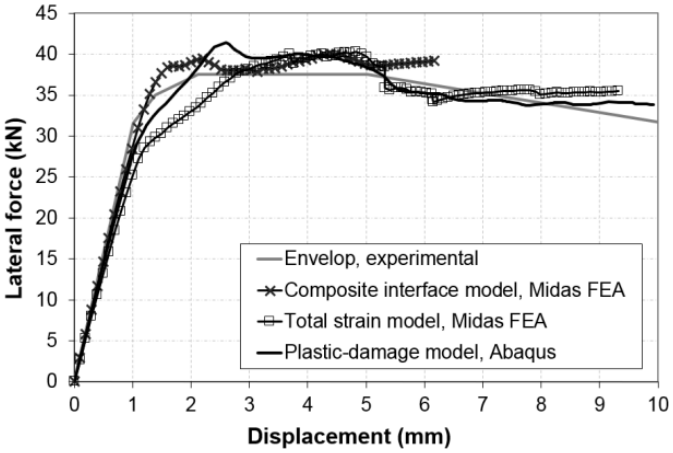

Fig. 12 Force-displacement curves: experimental results and numerical modelling

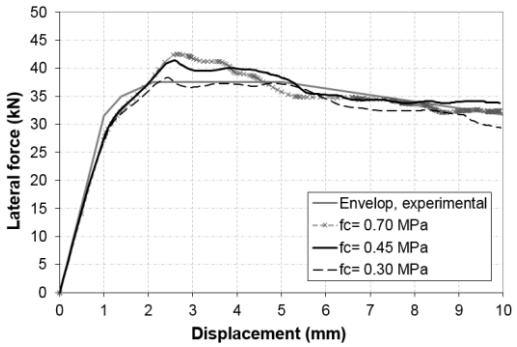

Fig. 13 Sensitivity of the adobe wall response to the variation of f_c (considering in all analyses f_t = 0.04 MPa, G^I_f = 0.01 N/mm & G_c/f_c = 0.344 mm)

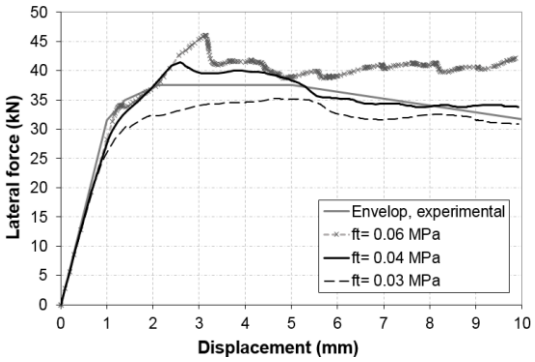

Fig. 14 Sensitivity of the adobe wall response to the variation of f_t (considering in all analyses f_c= 0.45 MPa, G_c/f_c= 0.344 mm & G^I_f = 0.01 N/mm)

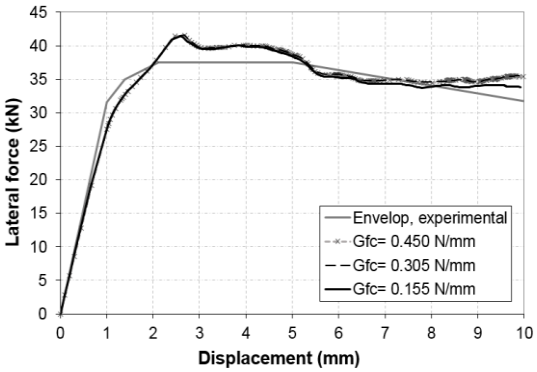

Fig. 15 Sensitivity of the adobe wall response to the variation of G_c (considering in all analyses f_c= 0.45 MPa, f_t = 0.04 MPa & G^I_f = 0.01 N/mm)

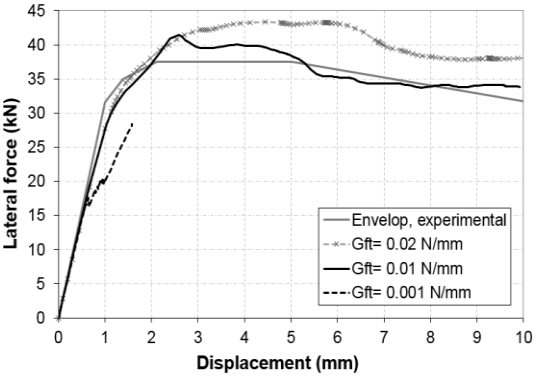

Fig. 16 Sensitivity of the adobe wall response to the variation of G^I_f (considering in all analyses f_c= 0.45 MPa, G_c/f_c= 0.344 mm & f_t = 0.04 MPa)

As it is well known, the response of quasi brittle materials is more sensitive to the variation of the tensile strength than to the variation of the compressive strength. To study the influence of the strength, additional analysis were done considering values of f_c varying from 0.30 to 0.70 MPa, with a fracture energy proportional to the corresponding for f_c= 0.45 MPa (i.e., G_c/f_c= 0.344 mm). This comparative analysis was performed with the plastic-damage modeland the results are shown in Fig. 13. It is seen that the compressive strength influences the maximum lateral strength of the adobe wall, though it does not affect the post peak behaviour and failure pattern; which is controlled in part by the fracture energy. The main differences in terms of lateral strength are seen between 2 and 4 mm of top displacement. A lower difference is seen for the pushover curves computed with f_c=0.45 to 0.70 MPa.

Another sensitivity study was carried out varying the tensile strength (between 0.03 and 0.06 MPa), keeping the tensile fracture energy at 0.01 N/mm and the compressive strength at 0.45 MPa. The analyses were carried out with the plastic-damage model, and the results are shown in Fig. 14, proving the pronounced influence of the tensile strength on the wall response. Increasing the material tensile strength induces an increase in the lateral strength and a concentration of the damage in the adobe wall diagonal. On the other hand, for lower values of tensile strength the damage is more distributed in the adobe wall, representing better the damage pattern observed in the test (Fig. 3d).

The last sensitivity analysis intended to assess the influence of the compressive and tensional fracture energy in the response of the adobe wall. The results presented in Fig. 15 indicates the low influence of G_c on the global response even increasing this value up to 3 times. This means that more important than the compressive fracture energy is the initial and maximum compressive strength. Instead, the results presented in Fig. 16 show a significant wall strength variation in contrast to the measured in the experimental test, pointing out the importance of a correct definition of the tensile fracture energy to properly represent the behaviour of adobe masonry walls. A lower value of G_f^I induces a more brittle behaviour of the adobe masonry without any energy dissipation capacity.

5.2 Cyclic seismic response

In this section, the finite element model created with the plastic-damage model was upgraded for the representation of the cyclic behaviour through the calibration of the damage factors in tension d_t and in compression d_c, and the stiffness recovery values w_t and w_c, for tension and compression, respectively (see Fig. 7). The damage factors control the cracking closing and the unloading stiffness. The values of the tensile and compressive strengths, and its respective fracture energies, are specified in Table 3.

In the concrete damaged plasticity model, supported by experimental tests, it is considered that after concrete cracking the compressive stiffness is recovered upon crack closure when the load changes from tension to compression. On the other hand, in the implemented model the tensile stiffness is not recovered when the load changes from compression to tension once crushing micro-cracks have developed in compression. These modelling assumptions are taken for the adobe masonry simulation.

The finite element model created for this analysis is similar to the one showed in Fig. 8b (4-node shell elements). Unlike the previous model, the displacement load is applied at both vertical edges of the concrete beam (top of the wall) for simulating the cyclic loading. The history of

imposed lateral displacements consisted of one cycle of ±1,±2, ±5 and ±10 mm. For convergence control just an automatic stabilization of 0.0002 is selected.

5.2.1 Calibration of damage factors (d_t and d_c) and stiffness recovery values (w_t and w_c)

Since no experimental data exist concerning the mechanical characterization of adobe masonry under reversal loads in tension and compression, stiffness recovery values (w_c and w_t) and damage factors (d_t and d_c, see Fig. 7) are proposed to consider its influence in the adobe structures response (Tarque 2011). The idea is to represent numerically the effect of the cracks closing during the transition from tension to compression stress with calibrated damage factors, which varies between 0 and 1. With the best adopted values for these parameters (Table 4), the force-displacement curves obtained with the numerical models are compared with the results of the cyclic test.

By default, Abaqus/Standard assumes w_c= 1 and w_t= 0, which represents full stiffness recovery when in the integration point is installed compression stresses, and no stiffness recovery when tensile stress is installed. For adobe masonry, w_c between 0.5 and 0.6 give good representation of the behaviour under reversal loads, here a w_c= 0.5 is used. Major attention has been put to the tensile behaviour, in contrast to the compressive, since the tension stress controls the global in-plane response of adobe walls. The calibrated tensile damage factors (d_t) are showed in Table 4.

As graphically represented in Table 4, it is not reached zero crack displacement when the load passes from tension to compression, even with large values of tensile damage factors. So, a residual crack aperture appears for reversal loadings and this effect will be reflected in the numerical cyclic curve response (see Fig. 18). In Table 4, the crack displacement values presented are equal to the crack tensile strain times the characteristic element length (h= 141 mm).

An alternative way for the identification and interpretation of the tensile damage occurred in the adobe masonry at the end of the analysis is evaluating the tensile damage factor distribution (Fig. 17). The tensile damage factor is a non-decreasing quantity associated with the tensile failure of the material. In Fig. 17, the grey zones indicate the regions which already are in the softening branch of the tensile constitutive law, that and can be considered as damaged zones.

Here, the numerical formation of X-diagonal cracks is evident, as typical for adobe masonry walls cyclically loaded in-plane. However, due to the geometric non linearity specified in the model and the degradation of the adobe material -even at early steps- the failure pattern is not symmetric at all for cyclic loading, similar results were seen in the test (Fig. 3c). So, the numerical results obtained here reproduced quite well the global failure pattern observed in the experimental test (Fig. 3d).

5.2.2 Global force-displacement response

The material properties given in Table 3 and the tensile damage factors proposed in Table 4 are result of the iterative calibration process, matching quite well the numerical results with the experimental ones in terms of strength, lateral capacity and crack pattern. These proposed material properties for numerical models is an important contribution of this research, since there is not available a complete experimental database for the adobe material properties. Here the compressive strength value should be interpreted as a lower bound, leaving the possibility to use higher values. Comparing the numerical and experimental pushover curves, it is observed an acceptable agreement for the loading branches and acceptable agreement is achieved for the cyclic reversal demands (Fig. 18). When the load changes sign, from positive to negative and vice versa,

the numerical results does not follow the experimental curve at the first load steps, showing larger deformations due to the incapacity of representing the complete closing of the tensile cracks. This fact results in an overestimation of the energy dissipation and could be solved modifying the damage plasticity law specified in continuum models to take into account the pinching effect.

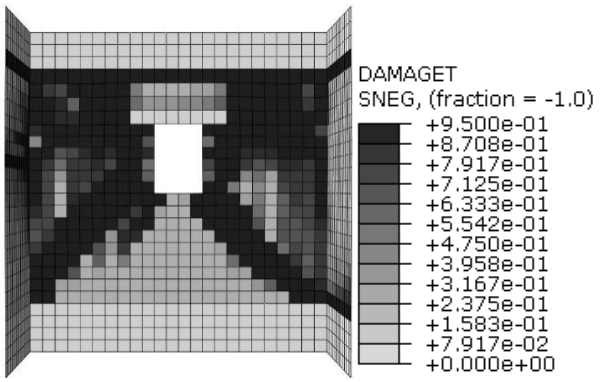

Fig. 17 Damaged zones in tension at the end of the cyclic loading demand (middle shell surface)

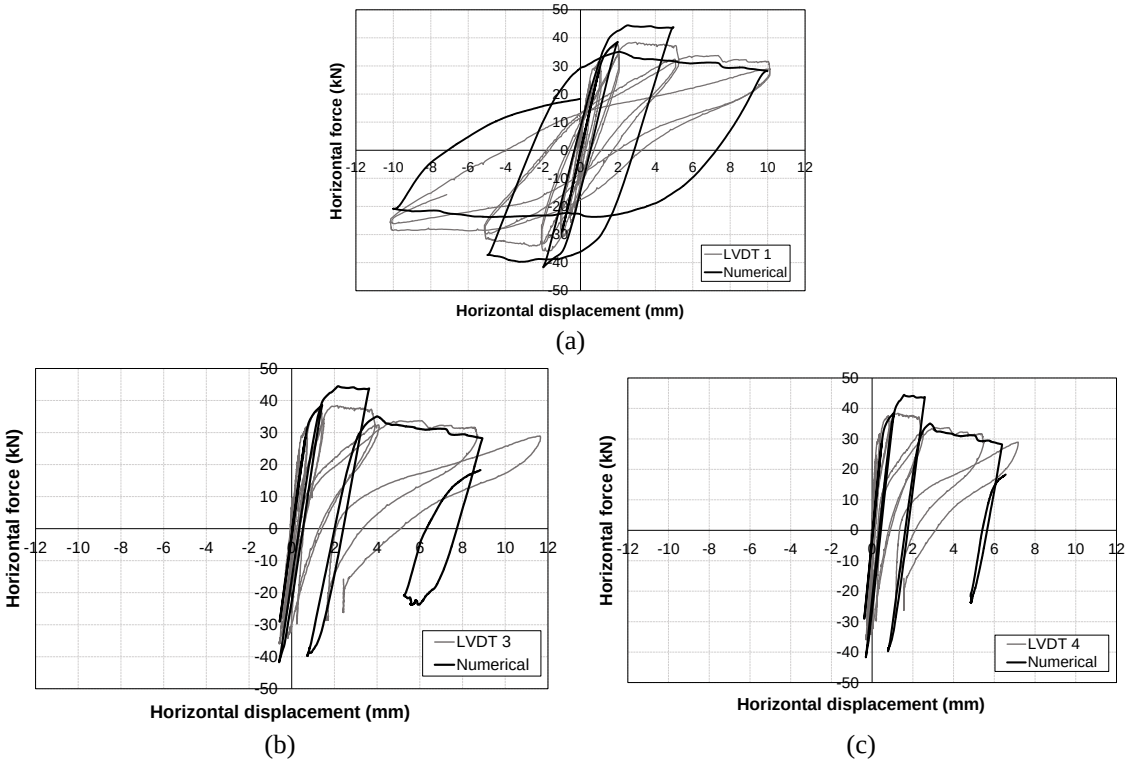

Fig. 18 Comparison between the experimental and numerical force-displacement response for the cyclic demand: (a) wall top LVDT 1, (b) middle part of the window (LVDT 3), (c) bottom part of the window (LVDT 4).

Table 4 Proposed tensile damage factor

Damage factor dt	Plastic disp. (mm)
0.00	0.000
0.85	0.125
0.90	0.250
0.95	0.500

Graphical representation of the degradation stiffness

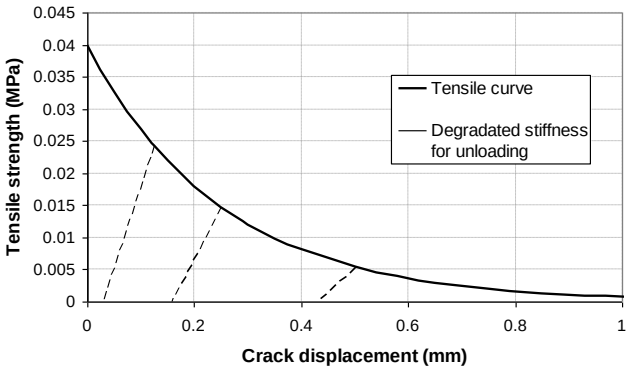

6. Conclusions

This paper focuses on the numerical analysis of the response of an adobe wall, previously tested under cyclic loads. Due to the lack of a full experimental database for the characterization of the adobe material properties (brick and mortar), the main objective of this work was the calibration of material properties (i.e., tension, compression and shear) in order to reproduce numerically the in-plane seismic response of the tested adobe wall.

For the monotonic analysis, three numerical models were created. The first considered the nonlinearity at the mortar joints (discrete crack model, simplified micro-modelling), and the other two considered the nonlinearity smeared over the FE mesh (total-strain and concrete damaged models, macro-modelling).All three models were able to reproduce with good accuracy the in-plane response of the tested adobe wall, including the crack initiation and propagation. In what regards convergence issues, the distributed (smeared) model used in this study showed a more stable numerical behaviour.

Using the smeared crack approach, a parametric study was performed in order to demonstrate the limited influence of the compressive strength and the major influence of the tensile strength on the global behaviour of adobe walls loaded in-plane. More specifically, for the more stable continuum model analysis, the compressive strength for the adobe masonry was taken as 0.45 MPa with a ratio G_c/f_c = 0.344 mm, and the tensile strength, f_t, as 0.04 MPa with G_f= 0.01 N/mm. Furthermore, the cyclic response of the adobe wall was reproduced and for this the damage factors for tensile behaviour were calibrated to match quiet well the global behaviour (damage pattern) and the experimental force-displacement curve (capacity).

The lack of experimental data for the evaluation of the hardening/softening behaviour of the adobe composite material (brick and mortar) introduces uncertainties in the numerical modelling of the adobe structures' response. Even though, the material properties calibrated and used in this work represent well the experimental behaviour of the tested adobe wall, there is a strong need extensive experimental campaigns aimed at characterizing the mechanical properties of different adobe materials and construction techniques. Provided additional material test data is available, numerical analyses such as those presented in this paper may be used to gain insight on the seismic behaviour of different adobe structures.

References

Abaqus 6.9 SIMULIA (2009), Abaqus/CAE Extended Funcionality EF2, Manual. Dassault Systemss Corporation, Providence, RI, USA.

Blondet, M., Torrealva, D., Villa-García, G. and Ginocchio, F. (2005), Reforzamiento de construcciones de adobe con elementos producidos industrialmente: estudio preliminar (in Spanish), Report DAI 113.0225, Catholic University of Peru, Lima, Peru.

Blondet, M. and Vargas, J. (1978), *Investigación Sobre Vivienda Rural* (In Spanish), Report, Division of Civil Engineering, Catholic University of Peru, Lima, Peru.

Calderini, C. and Lagomarsino, S. (2008), "Continuum model for in-plane anisotropic inelastic behaviour of masonry", *ASCE J. Struct. Eng.*, **134**, 209-220.

Cruz, J.S., Barros, J. and Azevedo, Á. (2004), *Elasto-Plastic Multi-Fixed Smeared Crack Model for Concrete*, Report 04-DEC/E-05, University of Minho, Minho, Portugal.

Gambarotta, L. and Lagomarsino, S. (1997), "Damage models for the seismic response of brick masonry shear walls. Part II: The continuum model and its applications", *Earthq. Eng. Struct. Dyn.*, **26**(4), 441-462.

Giordano, A., Mele, E. and De Luca, A. (2002), "Numerical modelling of masonry structures through different approaches", Ph.D. Thesis, University Federico II, Naples, Italy.

Lagomarsino, S., Penna, A., Galasco, A. and Cattari, S. (2013), "TREMURI program: an equivalent frame model for the nonlinear seismic analysis of masonry buildings", *Eng. Struct.*, **56**, 1787-1799.

Lee, J. and Fenves, G.L. (1998), "Plastic-damage model for cyclic loading of concrete structures", *J. Eng. Mech.*, **124**(8), 892-900.

Lotfi, H.R. and Shing, P.B. (1994), "Interface model applied to fracture of masonry structures", *J. Struct. Eng.*, **120**(1), 63-80.

Lourenço, P.B. (1996), "Computational strategies for masonry structures", Ph.D. Thesis, Delft University, Delft, The Netherlands.

Lowman, P.D. and Montgomery, B.C. (1998), Preliminary determination of epicenters of 358, 214 events between 1963 and 1998. <http://denali.gsfc.nasa.gov/dtam/seismic/>.

Lubliner, J., Oliver, J., Oller, S. and Oñate, E. (1989), "A plastic-damage model for concrete", *Int. J. Solids Struct.*, **25**(3), 299-326.

Magenes, G. and Della Fontana, A. (1998), "Simplified non-linear seismic analysis of masonry buildings", *Proceedings of Fifth International Masonry Conference*, British Masonry Society, London, England.

Midas FEA v2.9.6. (2009), Nonlinear and Detail FE Analysis System for Civil Structures. Manual: Analysis and Algorithm. CSP FEA.

Ngo, D. and Scordelis, A.C. (1967), "Finite element analysis of reinforced concrete beams", *Am. Concrete Inst.*, **64**(3), 152-163.

Pelà, L., Cervera, M. and Roca, P. (2013), "An orthotropic damage model for the analysis of masonry structures", *Construct. Build. Mater.*, **41**, 957-967.

Roca, P., Cervera, M., Gariup, G. and Pelà, L. (2010), "Structural analysis of masonry historical constructions. classical and advanced approaches", *Archives Comput. Meth. Eng.*, 17, 299-325.

De Sensi, B. (2003), Terracruda, la diffusione dell'architettura di terra. www.terracruda.com/architetturadiffusione.htm, http://www.terracruda.com/architetturadiffusione.htm, <www.terracruda.com/architetturadiffusione.htm>.

Stavridis, A. and Shing, P.B. (2010), "Finite element modeling of nonlinear behavior of masonry-infilled RC frames", *J. Struct. Eng., ASCE*, **136**(3), 285-296.

Tarque, N. (2011), "Numerical modelling of the seismic behaviour of adobe buildings", Ph.D. Thesis, ROSE School, Istituto di Studi Superiori di Pavia IUSS, Pavia, Italy.

Tarque, N., Crowley, H., Pinho, R. and Varum, H. (2012), "Displacement-based fragility curves for seismic assessment of adobe buildings in cusco, Peru", *Earthq. Spect.*, **28**(2), 759-794.

Wawrzynek, A. and Cincio, A. (2005), "Plastic-damage macro-model for non-linear masonry structures

subjected to cyclic or dynamic loads", *Proceedings of Conference Analytical Models and New Concepts in Concrete and Masonry Structures*, AMCM'2005, Gliwice, Poland.

Webster, F. (2008), Earthen Structures: Assessing Seismic Damage, Performance, and Interventions.Chapter of In Terra Literature Review, An Overview of Research in Earthen Architecture Conservation. E. Avrami, H. Guillaud, and M. Hardy, eds., http://www.getty.edu/conservation/publications/pdf_publications/terra_lit_review.pdf, Los Angeles, California, USA, 69-79.

SA